ARTICLE

Graphene as Atomic Template and Structural Scaffold in the Synthesis of Graphene–Organic Hybrid Wire with Photovoltaic Properties

Shuai Wang,[†,§] Bee Min Goh,[†,§] Kiran Kumar Manga,[†] Qiaoliang Bao,[†] Ping Yang,[‡] and Kian Ping Loh[†,*]

[†]Department of Chemistry, National University of Singapore, 3 Science Drive 3, Singapore 117543 and [‡]Singapore Synchrotron Light Source (SSLS), National University of Singapore, 3 Science Drive 3, Singapore 117543. [§]These authors contributed equally to this work.

ABSTRACT The dual role of graphene (or reduced graphene oxide) as atomic template and structural scaffold in the nucleation and assembly of organic nanostructures is demonstrated. The $\pi-\pi$ stacking interactions between graphene and aromatic organic molecules affords synergistic binding interactions, with the host and guest assuming the interchangeable roles of atomic template and structural scaffold. Beginning with the seeding of organic wires on graphene template, the outgrown organic wires in turn act as one-dimensional scaffolds where graphene sheets coat around to form a unique graphene–organic hybrid structure. Using this π-assembly approach, we have synthesized one-dimensional hybrid structures consisting of graphene–*N*,*N*′-dioctyl-3,4,9,10-perylenedicarboximide (PDI) organic wires. This hybrid structure shows enhanced performance over its individual components in donor–acceptor type (PDI–Graphene/polythiophene) solar cells.

KEYWORDS: graphene · perylene · template-assisted assembly · wire · hybrid

Graphene is a fascinating material not just for electronic applications, but also for its use as a dispersible aromatic platform for chemical reactions. Research in graphene has now proceeded from the initial phase of developing myriad strategies for the synthesis of graphene sheets to the use of graphene as a precursor in catalysis[1] or chemical synthesis.[2] One possibility is the use of graphene as a templating agent for the synthesis of organic crystals. Conventional fabrication methods for one-dimensional (1D) organic nanowires are broadly categorized as either solution-based or templated self-assemblies.[3] Self-assembly of molecules can occur rapidly using a biphasic system because the phase transfer from "good solvent" to "poor solvent" causes instantaneous 1D self-assembly *via* cofacial $\pi-\pi$ stacking between the molecular skeletons in order to lower the surface free energy. In the template synthesis pioneered by Martin and co-researchers,[4] heterogeneous seeds (particles or surfaces) are used to promote crystallization.[5]

Many small organic molecules such as porphyrin and *N*,*N*′-dioctyl-3,4,9,10-perylenedicarboximide (PDI) tend to self-assemble *via* noncovalent interactions (hydrogen bonding, van der Waals, $\pi-\pi$ stacking, and electrostatics) to form nanostructures.[6−9] As opposed to assembly in a two-phase solvent system, molecular self-assembly on a template bears the potential for engineering much more advanced structures with a higher degree of complexity.[10,11] Controlled nucleation of a specific crystallographic phase can be achieved with polymorphic matching between host substrate and guest nuclei. In solution, the role of the substrate is more complicated because of its dynamic dispersion. For example, it can lower the nucleation energy and seed the formation of nanostructures. Another possibility is that due to complementary binding interactions, the atomic template can be incorporated into the self-assembled structure to become an integral part of the structural scaffold.

Here, we investigate whether graphene sheet can play the role of either the structural scaffold or atomic template for crystal growth. The differentiation between the two roles is subtle. The atomic template seeds the nucleation, but does not get incorporated into the assembled structure, whereas a structural scaffold acts as an integral structural component of the assembled system. It is possible that these roles are interchangeable by controlling the assembly chemistry, leading to the synthesis of graphene–organic hybrids with unique structure (Scheme 1).

*Address correspondence to chmlohkp@nus.edu.sg.

Received for review July 27, 2010 and accepted September 1, 2010.

Published online September 8, 2010.
10.1021/nn101800n

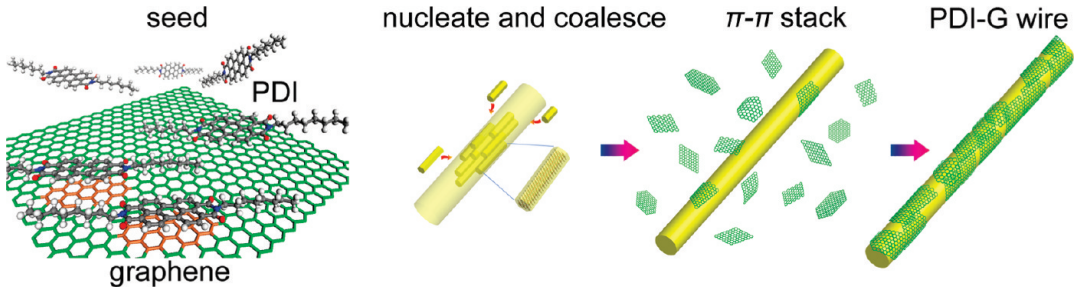

Scheme 1. Schematic diagrams illustrating the nucleation and growth of graphene-coated PDI wires (PDI−G wire).

To explore the cooperative π−π assembly between graphene and a planar aromatic molecule, we choose the perylene-based PDI as the organic molecule. The use of PDI is justified by its chemical robustness and high thermal stability and photostability which favor its usage in the fabrication of optoelectronic devices.[12,13] In addition, PDI is a crystalline *n*-type material which has higher electron mobility and exciton diffusion length than amorphous composites.[13−15] It can also be an alternative to C_{60}-PCBM in organic photovoltaics due to its relatively low cost.[15]

RESULTS AND DISCUSSIONS

PDI−G hybrids were prepared by hydrothermal treatment of graphene oxide (GO) and PDI in DMF. The starting material, GO, was characterized by atomic force microscopy (AFM). The AFM topographical image and size distribution curve (Figure 1a) reveal that the size of GO is in the range of 1−4 μm. By performing hydrothermal treatment at 180 °C, GO is readily reduced to G. Evidence of the deoxygenation of GO flakes can be obtained from solid state ^{13}C nuclear magnetic resonance (^{13}C NMR) (Figure 1b) and high resolution X-ray photoemission (XPS) analyses (Figure 1c,d). The ^{13}C NMR spectrum of GO before hydrothermal reduction shows peaks assignable to the hydroxyl group (C−OH) and epoxide (C−O−C) at 69 ppm and 60 ppm, respectively. The intensity of these peaks due to oxygenated groups becomes greatly reduced after hydrothermal treatment at 180 °C, and this is accompanied by an increase in peak intensity of sp^2 carbon (C═C) group at 100−143 ppm, which reflects the restoration of π conjugation of G (Figure 1b). XPS analysis (Figure 1c,d) also shows the occurrence of deoxygenation following hydrothermal treatment, as judged by the reduction in intensities of the chemically shifted peaks.

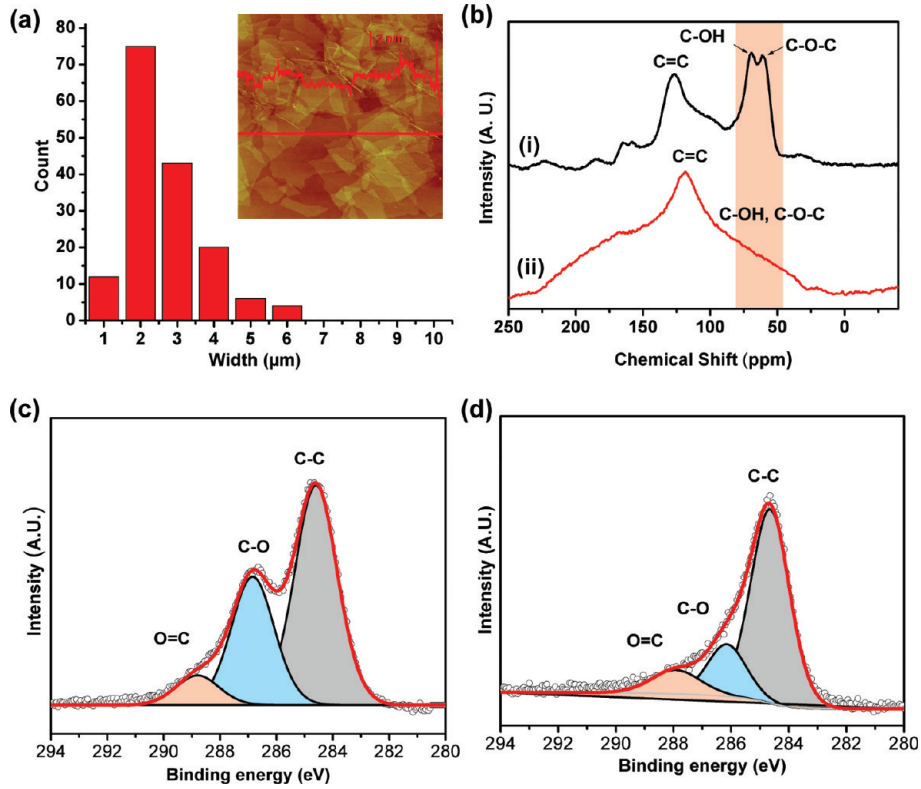

Figure 1. (a) AFM images (inset) and frequency counts of size distribution of GO. (b) ^{13}C solid state NMR spectra of GO before (i) and after (ii) hydrothermal treatment at 180 °C. (c, d) XPS spectra of GO before (c) and after (d) hydrothermal treatment at 180 °C.

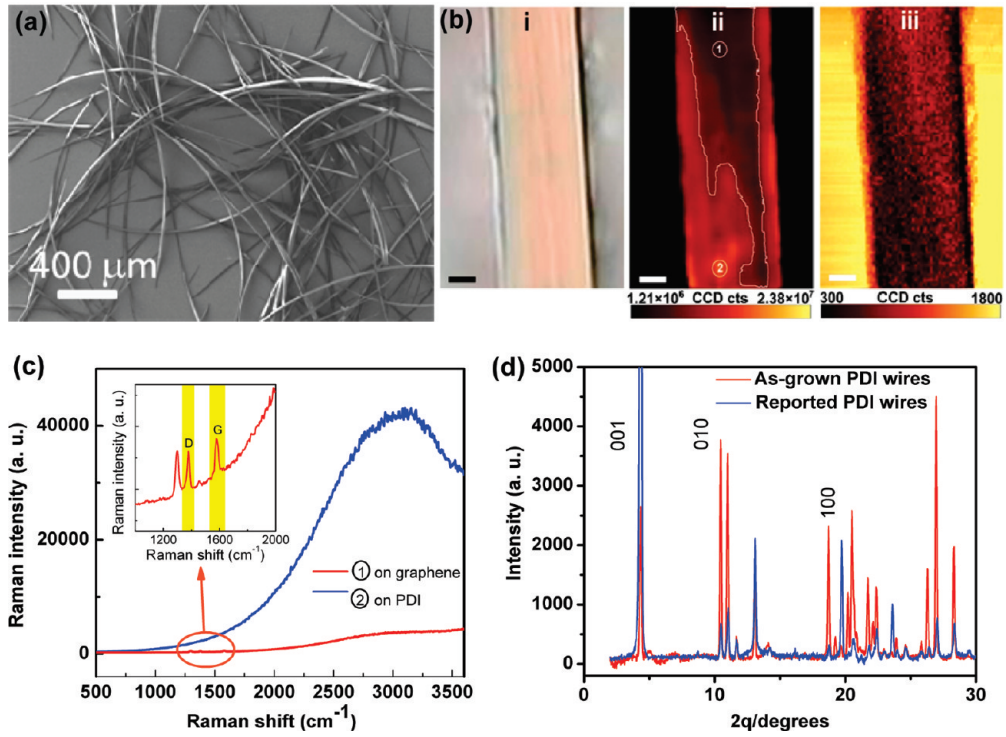

Figure 2. Characterizations of PDI−G wires. (a) SEM image of PDI−G wires obtained from PDI−GO 1:0.5 after hydrothermal treatment at 180°. (b) i, bright-field optical image; ii, photoluminescence map; and iii, fluorescence-corrected Raman map of the G band of graphene (excited by 532 nm laser). Scale bars: 2 μm. (c) Raman spectra taken from two different locations marked in panel b-ii. (d) XRD patterns of as grown PDI wires and reported PDI wires obtained from two-phase solvent method are shown for comparison.

The reduced GO flakes act as a seeding agent for PDI wire growth since no wires can form in DMF in the absence of GO. The synthesized wires have diameters in the range of 5−10 μm (Figure 2a and Supporting Information Figure S1). We infer that cooperative π−π stacking interactions are the main driving force for heterogeneous nucleation of the PDI molecules on these flakes, among other possible interactions such as hydrogen bonding with residual oxygen groups on reduced GO. It must be stated that similar nucleation effects for PDI are observed when other pure carbon-based structures possessing aromatic scaffold are used. We have tested fullerenes (C_{60}), single-walled carbon nanotubes (SWNT), and graphite flakes as seeding agents (Figure 3) and obtained PDI wires successfully in all cases, which underpin the importance of π−π interactions. The shape and size of the PDI wires grown may be different, due to the differences in size of the nucleation template.

It is difficult to observe the presence of atomically thin graphene on PDI wires using optical microscope because of its weak optical contrast (Figure 2b,i). In this case, the presence of reduced graphene oxide sheets attached to the PDI wires can be verified using fluorescence and Raman mapping, as shown in Figure 2b. It is well-known that metallic graphene quenches the fluorescence from organic dyes efficiently through energy transfer and forms the basis of the fluorescence quenching microscopy technique.[16] The relatively dark area surrounded by the white line in Figure 2b,ii indicates the area covered by the graphene flakes. Raman analysis of this region (Figure 2b,iii) reveals the fingerprint G band (1580 cm^{-1}) and D band (1380 cm^{-1}) of graphene. The peaks can be resolved against the fluorescent background because of the effective quenching of the fluorescence from PDI wires by more than 10 times, as shown in Figure 2c. To shed light on the structure of the PDI wire, X-ray diffracted analysis (XRD) was conducted. All the diffraction peaks can be indexed to the triclinic structure with constant lattice of $a = 4.69(5)$ Å, $b = 8.56(6)$ Å, $c = 20.0(2)$ Å, $\alpha = 86.28(1)°$, $\beta = 90.16(2)°$, and $\gamma = 81.96(1)°$ (Figure 1d). The XRD data reveal that the fabricated PDI wires are highly crystalline.[17] The crystallinity of the fabricated organic wires is similar to that of PDI wires grown from phase transfer method, as judged from the comparative XRD spectra in Figure 2d. However, the graphene template-assisted method yields better textural characteristic than the PDI wires fabricated by the conventional two-phase solvent method. As shown in Figure 2a, the PDI wires fabricated by template-assisted assembly are extremely long and exhibit uniform-width diameter.

Arising from the use of these different seeding agents, a range of PDI nanostructures with different morphologies can be produced, as shown in Figure 3. Interestingly, the use of C_{60} as the seeding template produces 1-D microbelts (Figure 3a). When 1-D single-walled carbon nanotube (SWNT) is used for seeding,

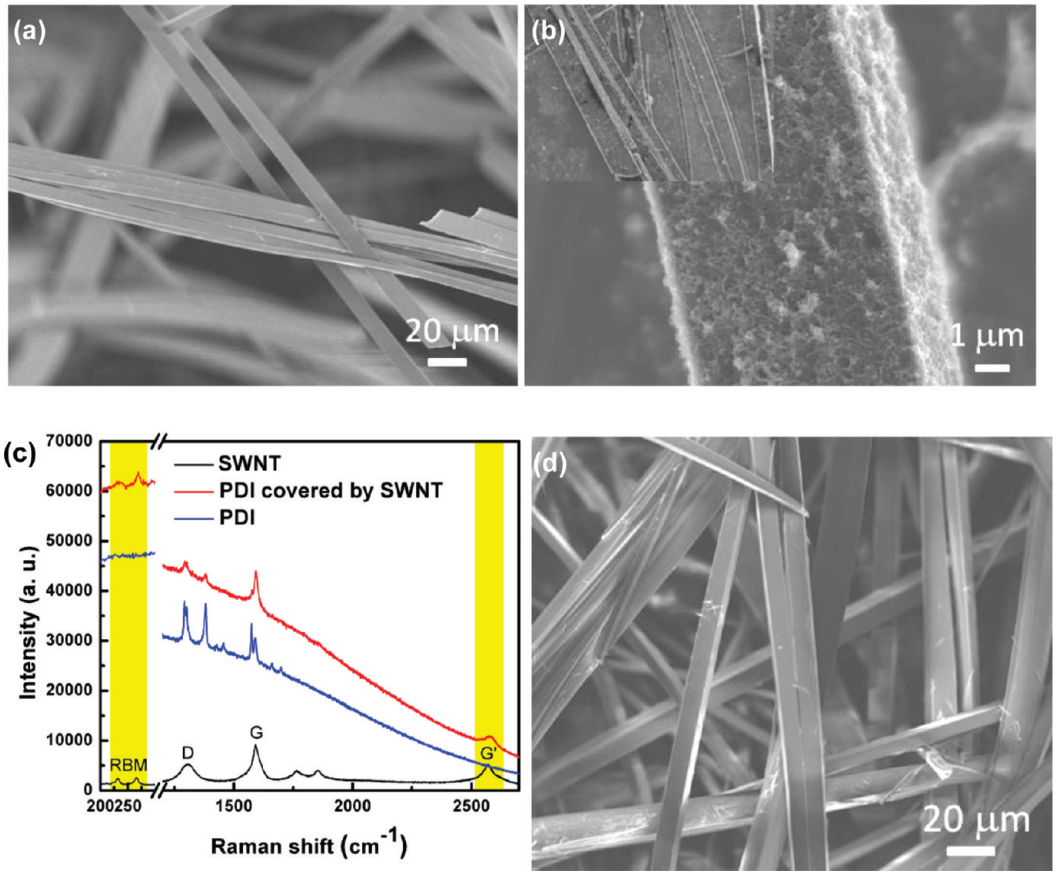

Figure 3. (a) SEM image 1D PDI microbelts seeded by fullerene template. (b) SEM image showing single-walled carbon nanotube (SWNT) covering the outer layer of 1D microbelt seeded by 1D SWNT template. Inset: The top-down image showing 1D PDI wires covered by SWNT. (c) Raman spectrum of SWNT-PDI microbelts (excited by 785 nm laser). The Raman spectra of pure SWNT and PDI are shown for comparison. (d) SEM image of 1D PDI wires seeded by graphite.

1-D PDI microbelts which are coated by SWNT are fabricated. 1-D PDI wire can be obtained by using graphite flakes as seeding agents, but in this case, the diameter of the wire is larger (in the range of 10−20 μm) than that obtained by using GO or G as the seeding agent. This is consistent with the kinetically controlled template model where a large size template acts as the boundary surface for nucleating large wires. These different microstructures which were produced by different types of nucleating agent used suggest that the surface area of template influences not just the size but also the shape of the nucleated products. The presence of adsorbed seeding agents on the growing organic wires suggests that the nucleating agent may transform into a growth inhibitory agent at a later stage of the growth process owing to surface passivation effects. For example, once the flat surface of any growing crystals reaches micrometer length in lateral scale, nanosized C_{60} or SWNT can bind readily to the flat face of these growing crystals and inhibit growth in the vertical direction, although the growth in the thinner horizontal direction is not impeded. A tape-like structure will ultimately evolve (Figure 3b). Evidence for the attachment of SWNT on the PDI microbelts is obtained from Raman analysis of the microbelts, as shown in Figure 3c. The Raman spectrum of PDI nanobelts covered by SWNT shows characteristics which are typical of both SWNT and PDI. The radial breathing mode and G′ mode (marked in yellow regions) of SWNT are clearly resolved. The high-frequency *Ag* breathing modes[22] of PDI at 1382, 1293 cm^{-1} are also observed. The G mode of SWNT at 1590 cm^{-1} and *Ag* breathing modes[21] of PDI at 1572 and 1591 cm^{-1} are overlapped and result in a Raman peak at 1593 cm^{-1} with a shoulder at 1576 cm^{-1}.

The graphene sheets or graphite platelets (Figure 3d) have microsized lateral faces which are larger than the nucleating wires in the initial growth phase, so the growing wires are not passivated by these seeding agents until its size exceeds that of graphene. In this case the growth of the nanostructure is isotropic in the radial direction, resulting in the growth of cylindrical wires. Therefore, depending on the size of the nucleating agent relative to that of the growing crystal, the role of host (atomic template) and guest (adsorbate) can interchange, mediated by π−π interactions.

An elegant illustration of this interchangeable role of atomic template and structural scaffold can be observed in the experiment where the sudden appearance of PDI in a solvent requires surface stabilization. A 1 mL aliquot of PDI−chloroform solution (0.7 mg/mL)

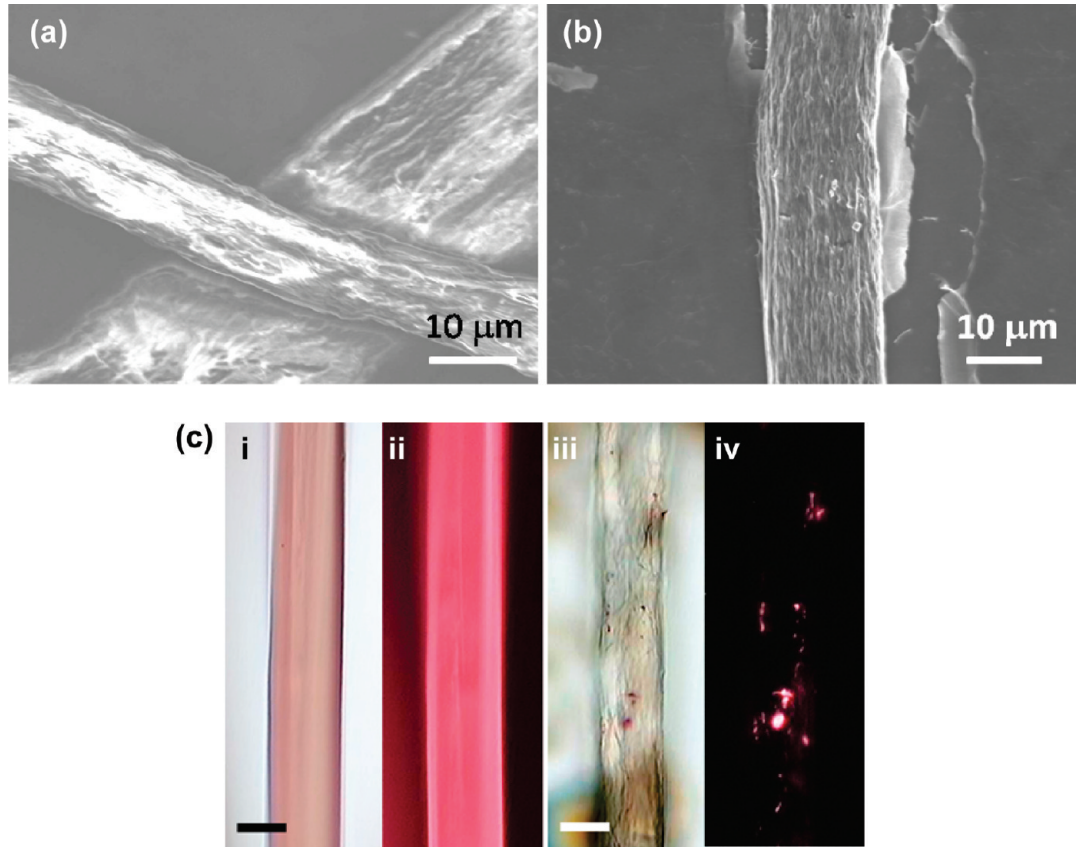

Figure 4. SEM and optical images of PDI−G coated with high density of G sheets. (a) SEM image of the PDI/GO core−shell structures. (b) SEM image showing the carbon shell after thermal annealing in vacuum at 1000 °C. (c) Bright-field optical images (i, iii) and corresponding dark-field photoluminescence microscopy images (ii, iv): (i, ii) PDI wires; (iii,iv) PDI−G hybrid. Scale bars: 10 μm.

was injected into 9 mL of large sized GO (0.08 mg/mL) sheets dispersed in a water/methanol mixture. The rapid growth and sudden appearance of the PDI wire in these double-phase solvent conditions induce the GO sheets to coat densely around the wire, due to the stabilization of the PDI wires by the hydrophilic GO. Figure 4a shows dense GO sheets coating around the PDI wire. To investigate the coverage of GO on PDI wires, the sample was subjected to gradual thermal annealing in vacuum. From the SEM images shown in Figure 4b, a carbon shell remains after the evaporation of the organic core, which suggests that the wrapped-around GO sheets are stable enough to act as structural scaffold. The wrapped-around GO−PDI hybrid wire can be converted to PDI−G wires using chemical reduction or heating.[18]

PL analysis of the reduced GO-wrapped PDI wires (abbreviated as PDI−G) synthesized here reveals effective quenching of fluorescence originating from the PDI wire, as shown in Figure 4c. 1-D PDI wire shows strong red light emission under green light. For the PDI−G wire, the photoluminescence originating from the PDI wire is effectively quenched when a high density of reduced GO sheets coat the PDI wire. The luminescent red spots in Figure 4c,iv are due to the attachment of small PDI particles on the reduced GO surface. These PL results show that photoexcited carriers in the organic wire can be transferred rapidly to the reduced GO sheets coating around it. We hypothesized that in the presence of reduced GO sheets forming an extended coating, that is, structural scaffold around the PDI wire, the resulting heterostructures should facilitate effective charge injection from the organic wire to the reduced GO sheets, which act as a carrier sink.

The photovoltaic properties of the PDI and G hybrids were investigated to determine whether they offer enhanced performances over that of the individual constituents like PDI and G. We also investigated the performance of physically mixed PDI + G composites which are made of discrete PDI and G—this system is used as a control to compare with the PDI−G hybrid

TABLE 1. Solar Cell Characteristics of G and PDI Hybrid[a]

composites	V_{oc} (V)	J_{sc} (mA/cm^2)	FF (%)	η (%)
PDI	0.49	0.78	16.7	0.064
PDI−G mixture[b]	0.90	0.013	18.0	0.002
PDI−G hybrid wires[c]	0.78	3.85	35	1.04

[a] V_{oc}, open circuit voltage; J_{sc}, short circuit current density; FF, fill factor; η, solar cell efficiency. [b] PDI−G were prepared by physically mixing PDI and G at a mass ratio of 1:10. [c] PDI−G hybrid wires were synthesized by the hydrothermal method with PDI and GO at a mass ratio of 1:0.5. PDI−G hybrids consist of reduced graphene oxide-wrapped PDI wires.

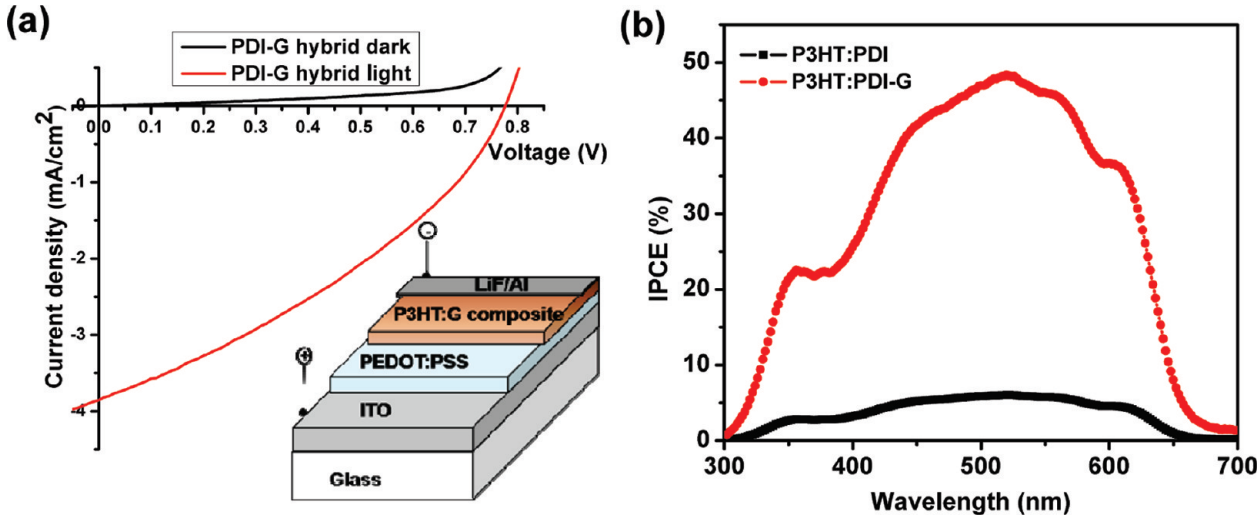

Figure 5. The enhanced performances of the PDI and G hybrids over that of the individual constituents like PDI and G on the application of organic solar cells. (a) Solar cell data: *I*−*V* plot of ITO/PEDOT:PSS/P3HT:PDI−G hybrid at 1:1 ratio/LiF/Al device under dark(black) and light(red) illumination after heating at 160 °C. Inset: Solar cell device structure. (b) IPCE spectra for PDI and PDI−G hybrid.

wires—in order to find out if the coating of G around the PDI wires offers any enhanced performance. Using a donor−acceptor type heterojunction cell structure, solar cells with an area of 11 mm^2 are fabricated from P3HT:PDI-based material films and tested using 100 mW/cm^2 AM 1.5 illumination.

The photovoltaic parameters, short-circuit current density (J_{sc}), open circuit voltage (V_{oc}), fill factor (FF), and power conversion efficiency (PCE) are provided in Table 1. Obviously, the PDI−G hybrid wires are far superior in all performance parameters compared to pure PDI and PDI−G mixture. There are improved current density values (3.85 mA/cm^2) and power conversion efficiency (1.04%) obtained for PDI−G hybrid wires compared to control PDI (0.78 mA/cm^2 and 0.064%) and physically mixed PDI−G composite (0.013 mA/cm^2 and 0.002%), as shown in Table 1. The vastly improved performance can be explained by the efficient exciton dissociation at the P3HT and PDI−G hybrid interface, as well as efficient charge transport enabled by the conjugated network of the graphene shells surrounding the PDI core. The device structure and current density−voltage characteristics of PDI−G hybrid devices are shown in Figure 5a. The incident-photon-to-electron conversion efficiency (IPCE) spectrum in Figure 5b reflects a broad band photocurrent conversion between 300 and 630 nm. The significant increase in IPCE for PDI−G wires compared to PDI alone proves the efficient charge injection and charge transport in PDI−G hybrid system. Further improvement can be obtained by optimizing the interface morphology between donor and acceptor moieties by controlled synthesis of thin hybrid wires.[19]

CONCLUSIONS

We have demonstrated that graphene can act as an effective nucleating agent for the growth of organic nanostructures. The validity of this approach extends to other forms of nanocarbon which possess the aromatic skeleton. Interestingly, it was observed that the perylene wire can be coated by graphene oxide or reduced graphene oxide sheets to form a hybrid system. Such type of synergistic interaction between organic nanostructures and nanocarbon affords a novel route to the synthesis of hybrid materials with new properties. We envisage that a new class of graphene−organic hybrids with applications in organic photovoltaics, optical waveguide, and sensors can be fabricated using this approach.

METHODS

Synthesis of PDI−G Wires. GO was prepared according to the method reported by Hummers.[20] The as-made GO sheets were dispersed in DMF (HPLC grade) at a concentration of 1 mg/mL^{-1} and ultrasonicated. PDI (Sigma Aldrich) was added into GO solution with a GO-to-PDI mass ratio of 1:2. The mixture was refluxed in a round-bottom flask under constant magnetic stirring at 80 °C for 24 h. Subsequently, the composite was washed with DMF/ethanol (1:5) by centrifuging at 11500 rpm until all unreacted PDI had been removed. PDI−G wires can be recovered from the synthesized composites. The PDI−GO composites were dried in a vacuum desiccator and dissolved in DMF at a concentration of 0.5 mg/mL. The PDI−GO composites can be hydrothermally reduced to PDI−G by transferring 40 mL of PDI−GO solution to a Teflon-lined stainless steel autoclave and then heated in a furnace for 24 h at 180 °C to produce PDI−G wires. The synthesized products were filtrated and washed with DMF to remove the unreacted PDI. All the synthesized materials were kept in vacuum desiccators. C_{60}, SWNT, and graphite were also used as nucleating seeds for the growth of PDI hybrid wires.

Synthesis of PDI−GO Hybrid. A 1 mL portion of PDI chloroform solution (0.7 mg/mL) was injected into 9 mL of big-sized GO (0.08

mg/mL)[21] dispersed in a water/methanol mixture with a ratio of 1:5. The PDI−GO hybrids were filtered and washed, and GO-wrapped PDI wires were found. The PDI−GO wires can be converted to PDI−G wires by hydrothermal reduction or thermal annealing.

Annealing of PDI−GO Hybrid. The PDI−GO hybrids are subjected to vacuum annealing in a temperature programmed oven with background pressure of 1×10^{-6} bar. The heating rate is set at 25 °C/min. These structures are heated up to 1000 °C for 1 h.

Solar Cell Device Fabrication and IPCE Measurement. P3HT, PDI, and graphene composites were mixed in a 1:1 ratio in dichlorobenzene (DCB) and spin-coated at 800 rpm on an ITO/PEDOT electrode for 70 s. The assembled films were annealed at 160 °C for 10 min under N_2 atmosphere. Subsequently LiF(1 nm) and Al (100 nm) electrodes were evaporated on the films at 1×10^{-6} bar vacuum to complete the device fabrication. The $I-V$ curves were recorded using the solar simulator AMG 1.5 light source at an intensity of 100 mW/cm^2. The light source employed was a Newport 300 W xenon light source, controlled by a Newport Digital Exposure Controller, which simulates the solar light through an AM 1.5G sunlight filter. The incident light intensity was focused and calibrated to 1 Sun (100 mW/cm^2) with a standard Si solar cell (PV Measurements, USA). Action spectrum was recorded using a Newport 300 W xenon light source monochromated by a Newport Cornerstone 260 monochromator. The light intensity was measured by a calibrated Newport Si detector.

Acknowledgment. The authors thank NRF-CRP for support through Grant "Graphene and Related Materials and Devices" (R-143-000-360-281).

Supporting Information Available: Additional TGA, SEM, TEM, and optical images of PDI−G hybrid wires, AFM image and size distribution of BSGO, and characterization information. This material is available free of charge *via* the Internet at http://pubs.acs.org.

REFERENCES AND NOTES

1. Lightcap, I. V.; Kosel, T. H.; Kamat, P. V. Decorating Graphene Sheets with Gold Nanoparticles. *Nano Lett.* **2010**, *10*, 577–583.
2. Stankovich, S.; Dikin, D. A.; Dommett, G. H. B.; Kohlhaas, K. M.; Zimney, E. J.; Stach, E. A.; Piner, R. D.; Nguyen, S. T.; Ruoff, R. S. Reversible Basal Plane Hydrogenation of Graphene. *Nature* **2006**, *442*, 282–285.
3. Zang, L.; Che, Y.; Moore, J. S. One-Dimensional Self-Assembly of Planar π-Conjugated Molecules: Adaptable Building Blocks for Organic Nanodevices. *Acc. Chem. Res.* **2008**, *41*, 1596–1608.
4. Miller, S. A.; Young, V. Y.; Martin, C. R. Electroosmotic Flow in Template-Prepared Carbon Nanotube Membranes. *J. Am. Chem. Soc.* **2001**, *123*, 12335–12342.
5. Urbanus, J.; Laven, J.; Roelands, C. P. M.; ter Horst, J. H.; Verdoes, D.; Jansens, P. J. Template Induced Crystallization: A Relation between Template Properties and Template Performance. *Cryst. Growth Des.* **2009**, *9*, 2762–2769.
6. Jordan, B. J.; Ofir, Y.; Patra, D.; Caldwell, S. T.; Kennedy, A.; Joubanian, S.; Rabani, G.; Cooke, G.; Rotello, V. M. Controlled Self-Assembly of Organic Nanowires and Platelets Using Dipolar and Hydrogen-Bonding Interactions. *Small.* **2008**, *4*, 2074–2078.
7. Schenning, A. P. H. J.; Meijer, E. W. Supramolecular Electronics: Nanowires from Self-Assembled π−Conjugated Systems. *Chem. Commun.* **2005**, *26*, 3245–3258.
8. Elemans, J. A. A. W.; Van Hameren, R.; Nolte, R. J. M.; Rowan, A. E. Molecular Materials by Self-Assembly of Porphyrins, Phthalocyanines, and Perylenes. *Adv. Mater.* **2006**, *18*, 1251–1266.
9. Hoeben, F. J. M.; Jonkheijm, P.; Meijer, E. W.; Schenning, A. P. H. J. About Supramolecular Assemblies of π-Conjugated Systems. *Chem. Rev.* **2005**, *105*, 1491–1546.
10. Forrest, S. R. Ultrathin Organic Films Grown by Organic Molecular Beam Deposition and Related Techniques. *Chem. Rev.* **1997**, *97*, 1793–1896.
11. Witte, G.; Hanel, K.; Sohnchen, S.; Woll, C. H. Growth and Morphology of Thin Films of Aromatic Molecules on Metals: The Case of Perylene. *Appl. Phys. A* **2006**, *82*, 447–455.
12. Balakrishnan, K.; Datar, A.; Naddo, T.; Huang, J.; Oitker, R.; Yen, M.; Zhao, J.; Zang, L. Effect of Side-Chain Substituents on Self-Assembly of Perylene Diimide Molecules: Morphology Control. *J. Am. Chem. Soc.* **2006**, *128*, 7390–7398.
13. Schmidt-Mende, L.; Fechtenkötter, A.; Müllen, K.; Moons, E.; Friend, R. H.; MacKenzie, J. D. Self-Organized Discotic Liquid Crystals for High-Efficiency Organic Photovoltaics. *Science.* **2001**, *293*, 1119–1122.
14. Jones, B. A.; Ahrens, M. J.; Yoon, M.-H.; Facchetti, A.; Marks, T. J.; Wasielewski, M. R. High-Mobility Air-Stable n-Type Semiconductors with Processing Versatility: Dicyanoperylene-3,4:9,10-bis(dicarboximides). *Angew. Chem., Int. Ed.* **2004**, *43*, 6363–6366.
15. Dittmer, J. J.; Marseglia, E. A.; Friend, R. H. Electron Trapping in Dye/Polymer Blend Photovoltaic Cells. *Adv. Mater.* **2000**, *12*, 1270–1274.
16. Kim, J.; Cote, L. J.; Kim, F.; Huang, J. Visualizing Graphene Based Sheets by Fluorescence Quenching Microscopy. *J. Am. Chem. Soc.* **2010**, *132* (1)), 260–267.
17. Briseno, A. L.; Mannsfeld, S. C. B.; Reese, C.; Hancock, J. M.; Xiong, Y.; Jenekhe, S. A.; Bao, Z.; Xia, Y. Perylene Diimide Nanowires and Their Use in Fabricating Field-Effect Transistors and Complementary Inverters. *Nano Lett.* **2007**, *7*, 2847–2853.
18. Liang, Y.; Wu, D.; Feng, L.; Mullen, K. Dispersion of Graphene Sheets in Organic Solvent Supported by Ionic Interaction. *Adv. Mater.* **2009**, *21*, 1679–1683.
19. Huynh, W. U.; Dittmer, J. J.; Alivisatos, A. P. Hybrid Nanorod−Polymer Solar Cells. *Science.* **2002**, *295*, 2425–2427.
20. Hummers, W.; Offeman, R. Preparation of Graphitic Oxide. *J. Am. Chem. Soc.* **1958**, *80*, 1339.
21. Wang, S.; Ang, P. K.; Wang, Z.; Tang, A. L. L.; Thong, J. T. L.; Loh, K. P. High Mobility, Printable and Solution-Processed Graphene Electronics. *Nano Lett.* **2010**, *10*, 92–98.